Spectral properties of electrons in fractal nanowires

Alberto Hernando,* Miroslav Šulc, and Jiří Vaníček†

Laboratory of Theoretical Physical Chemistry, Institut des Sciences et Ingénierie Chimiques,
École Polytechnique Fédérale de Lausanne, CH-1015 Lausanne, Switzerland
(Dated: March 27, 2015)

In view of promising applications of fractal nanostructures, we analyze the spectra of quantum particles in the Sierpinski carpet and study the non-correlated electron gas in this geometry. We show that the spectrum exhibits scale invariance with almost arbitrary spacing between energy levels, including large energy gaps at high energies. These features disappear in the analogous random fractal—where Anderson localization dominates—and in the regular lattice of equally sized holes—where only two length scales are present. The fractal structure amplifies microscopic effects, resulting in the presence of quantum behavior of the electron gas even at high temperatures. Our results demonstrate the potential of fractal nanostructures to improve the light-matter interaction at any frequency, with possible applications, e.g., in the development of solar cells with a wide absorption spectrum, artificial photosynthesis, or nanometamaterials with tailored Fermi levels and band gaps, operating in a wide range of frequencies, and with extended operating temperature range.

New generation of materials, based on nanostructures, is showing its potential to revolutionise industry [1, 2]. In parallel, self-similarity properties of fractal structures have revised the way we manufacture antennas [3] and permitted the production of novel metamaterials [4, 5]. New materials and manufacturing techniques have enabled producing fractal circuits [6], porous media such as silicas or aerogels, where superfluid helium flows in a fractal environment [7], fractal-shaped clusters of nanoparticles formed by aggregation [8]; or even fractal snowflakes composed of graphene [9]. Additionally, one can find self-similarity in the electronic spectra of quantum systems, such as in Hofstadter's butterfly and in the fractal quantum Hall effect [10, 11]. Indeed, quantum fractals are drawing an increasing attention due to their intriguing properties and potential applications [12].

To describe the properties of a quantum particle in a fractal geometry (e.g., an electron trapped in a fractal-shaped nanowire), we first find the eigenstates of the particle's Hamiltonian $\mathcal{H} = \mathcal{T} + \mathcal{V}$, where $\mathcal{T}$ is the kinetic energy operator and $\mathcal{V}$ is the potential energy of an infinite well with the desired fractal boundaries. For the well, we have chosen the paradigmatic Sierpinski carpet, a fractal object studied in many different contexts [6, 13]. This carpet is constructed by subdividing a square into smaller copies of itself and by removing the central copy iteratively, as shown in Fig. 1. Each iteration is labeled with an integer G indicating the *generation* of the carpet. We study generations up to $G = 6$, starting from $G = 0$, which represents the square well. Quantum Hamiltonian for a particle of mass m in a fractal geometry can be written as $\mathcal{H} = \mathcal{T} + \mathcal{V} = -\frac{\hbar^2}{2m}\nabla^2 + V(\mathbf{q})$, where $V(\mathbf{q})$ is an infinite well potential with the shape of the accessible region in the carpet of generation G and side L. Without loss of generality, units of L for length, $\hbar^2/mL^2$ for energy and $k_B\hbar^2/mL^2$ for temperature (where k_B is the Boltzmann constant) are used when m, $\hbar$, or L are not shown explicitly. For any finite generation G, Sierpinski

carpet can be viewed as a polygonal billiard with rational angles, and therefore is an example of pseudointegrable systems discovered by Richens and Berry [14], who also studied the equivalent of the first generation of Sierpinski carpet, albeit with periodic boundary conditions. As for higher fractal generations, Katomeris and Evangelou studied properties of Sierpinski *lattices* [12]; we instead focus on the dynamics of quantum particles in a fractal Sierpinski *volume*, such as electrons in fractal shaped wires, which are not yet well understood.

To obtain the eigenenergies and eigenstates of $\mathcal{H}$, we have used two different diagonalization methods: the finite differences method (FDM) and imaginary-time nonuniform-mesh method (ITNUMM) [15]—see section I in Supplementary Material (SM) for details. The relative error in the eigenenergies computed with FDM grows linearly with the energy, whereas the error remains roughly constant for the ITNUMM. Thus, despite the error of the FDM being smaller than the error of ITNUMM for the lowest-energy states, it eventually becomes larger for high-energy states. As a consequence, ITNUMM is the preferred method if one is interested in energies of many states. Nevertheless, we have verified all our numerical results by evaluating the energies both with ITNUMM and FDM.

The spinless single-particle spectrum. Figure 1 shows the structure of the lowest-lying states from the zeroth to fourth generation ($G = 0$, 1, 2, 3 and 4. Generations $G = 5$ and 6 are not shown due to the limitations of image resolution.) As the fractal generation increases, the wavefunctions develop intricate structures on smaller and smaller scales, resulting in the exponential increase of the kinetic energy of the ground state ϵ_{gs} (Fig. 2a). This contribution to the energy affects equally also all excited states and manifests itself as a global shift of the energy spectrum for a given generation. Hence, the mode number function $\mathcal{N}$ (Fig. 2b) and energy levels ϵ (Fig. 2c) are comparable for all genera-
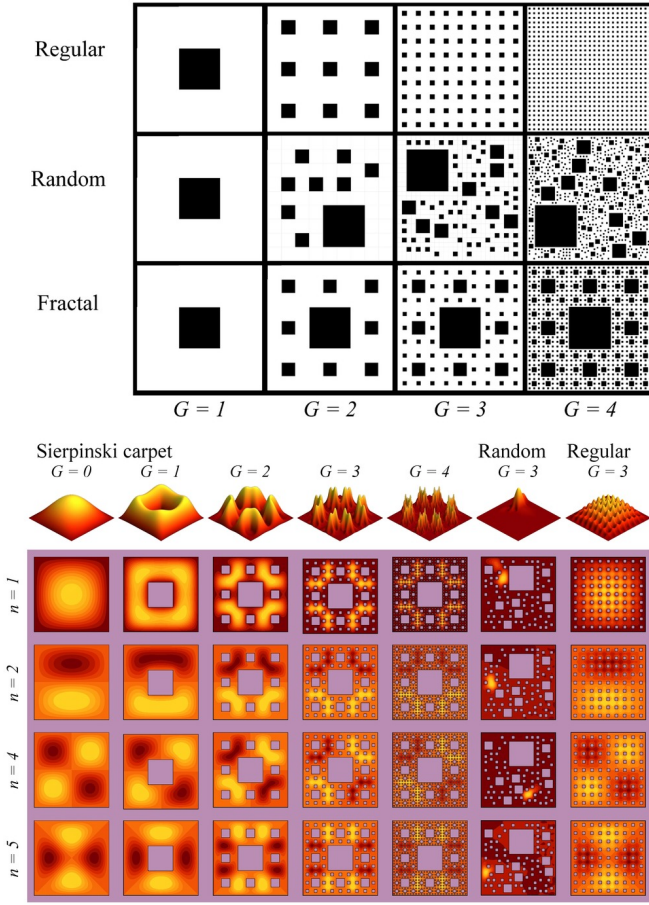
Figure 1. Top panel: Iterative procedure for constructing each generation G of the Sierpinski carpet ("Fractal"), and of the analogous random fractal ("Random") and regular non-fractal ("Regular") structures. Bottom panel: Wavefunctions of the first five states (rows $n = 1, 2, 4, 5$) for the particle in a box ($G = 0$), and for the first four generations of the Sierpinski carpet ($G = 1, 2, 3, 4$). For comparison, corresponding results are shown for the third generation ($G = 3$) of both the random fractal carpet (where Anderson localization takes place) and the regular non-fractal lattice.
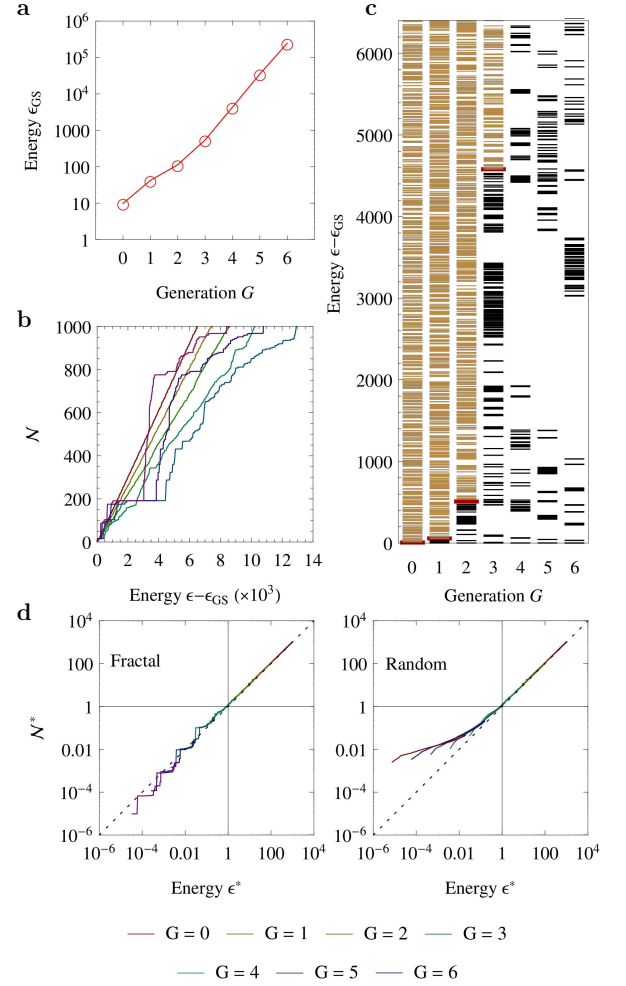

Figure 2. Spectrum of a single particle in a Sierpinski-shaped well. **a,** Ground state energy ϵ_{gs}: The exponential decrease of the smallest length scale with increasing generation G manifests itself in the exponential increase of ϵ_{gs}. **b,** Mode number function $\mathcal{N}(\epsilon - \epsilon_{gs})$. **c,** Energy level diagram: The border between low-energy, band-gap regime (black line segments) and the almost continuous high-energy regime (orange line segments) satisfying Weyl's law (see text) is shown for each G by a thick red line segment. **d,** The self-similarity of the spectrum becomes apparent when the energies and levels are rescaled according to Weyl's law (left panel: Sierpinski carpet; right panel: random carpet).

tions when referred to the ground state. For $G = 0$, one obtains the spectrum of a particle in a two-dimensional well [16], where the mode number is proportional to the energy as $\mathcal{N}(\epsilon) = \epsilon\, mL^2/2\pi\hbar^2$, as predicted by Weyl's law. Increasing the fractal generation gives rise to two qualitatively different energy regimes: (i) At lower energies, some levels attract each other, agglomerating into bands, while others exhibit repulsion, generating large gaps between the bands; (ii) at higher energies, the mode number eventually approaches the prediction of Weyl's law $\mathcal{N}(\epsilon) = \epsilon\, m^*L^2/2\pi\hbar^2$, where $m^* = (8/9)^G m$ is the effective mass. Using this analytical form to rescale mode numbers as $\mathcal{N}^* = \mathcal{N}/8^G$ and energies as $\epsilon^* = \epsilon mL^2/9^G 2\pi\hbar^2$ (see Fig. 2d, left panel), we find, remarkably, that *for any generation G* the bands and gaps in regime (i) appear in the part of the spectrum with

energies $\epsilon^* < 1$ ($\mathcal{N}^* < 1$), whereas the approximately constant density of states in regime (ii) appears for energies $\epsilon^* > 1$ ($\mathcal{N}^* > 1$). This scaling of the energy levels demonstrates that the self-similarity in the geometry is reflected also in a scale-invariant spectrum.

To further explore this phenomenon, we studied the eigenvalue nearest-neighbor spacing distribution in both regimes for all six generations. This distribution is widely used in the fields of random matrix theory and quantum chaos for characterizing ensembles of random matrices and dynamical properties of Hamiltonian sys-

tems [17, 18]. In addition, since the energy of any optical transition of an electron can be described as a sum of level spacings, their distribution can provide some information about the expected absorption/emission properties of fractal nanowires. After first unfolding the energy levels (as described in section II of the SM), we computed the spacings s of every two consecutive modes as well as the maximum likelihood estimates of the parameters α and b of the Brody distribution [19]

$$p(s) = (1 + b)\alpha s^b \exp\left(-\alpha s^{b+1}\right) \quad (1)$$

fit to the probability density of s. Whereas Brody distribution with zero Brody parameter ($b = 0$) reduces to the exponential distribution $p(s) = \alpha \exp\left(-\alpha s\right)$, reflecting Poisson level statistics characteristic of *generic integrable* systems [20], unit Brody parameter ($b = 1$) yields the Wigner distribution $p(s) = 2\alpha s \exp\left(-\alpha s^2\right)$ and, according to the quantum-chaos conjecture [21–24], reflects classically *chaotic* dynamics of systems with time-reversal invariant Hamiltonian. Generic time-reversal invariant systems with mixed dynamics and without symmetry can be well described with a mixture of exponential and Wigner distributions [24, 25]; while this mixture itself is not a Brody distribution, it can be typically well fitted with a Brody distribution with $0 < b < 1$. Remarkably, as shown in Fig. 3, for the Sierpinski carpet we find that the Brody parameter evolves from $b = -0.03 \pm 0.07$ for $G = 1$, corresponding to Poisson level statistics ($b = 0$), to $b = -0.96 \pm 0.03$ for $G \geq 6$ in regime (i), resulting in almost an inverse power law distribution ($b = -1$). As the generation increases, the level repulsion-attraction intensifies and it becomes harder to define the mean level spacing. Indeed, for the asymptotic value $b = -1$ the mean level spacing ceases to exist and the distribution cannot even be normalized; spacings of any order of magnitude are equally probable at any energy. This transition does not appear in regime (ii), where Brody parameter $b \approx 0$ in all the cases studied here. While transitions between non-negative Brody parameters (from $b = 1$ to $b = 0$) have been seen in the family of Koch fractals of changing fractal dimension [26], to the best of our knowledge a transition from Poisson statistics to a long-tailed distribution, similar to the one described here, was previously observed only by Katomeris and Evangelou, who saw a power law distribution with exponent -1.56 in a fractal lattice by removing diagonal disorder [12]. However, negative Brody parameters were observed previously in superintegrable systems ($b \approx -0.24$) [27] or 1D lattices with unbounded quantum diffusion ($b = -3/2$) [28]. For the desymmetrized system (see SM section II), we find a qualitatively similar behavior involving a transition from positive to negative values, confirming that the effect is due to the fractal geometry and not due to degeneracies from simple geometrical symmetries.

This peculiar feature of the spectrum of the Sierpinski carpet disappears (Fig. 3 and SM Fig. 9) both in the
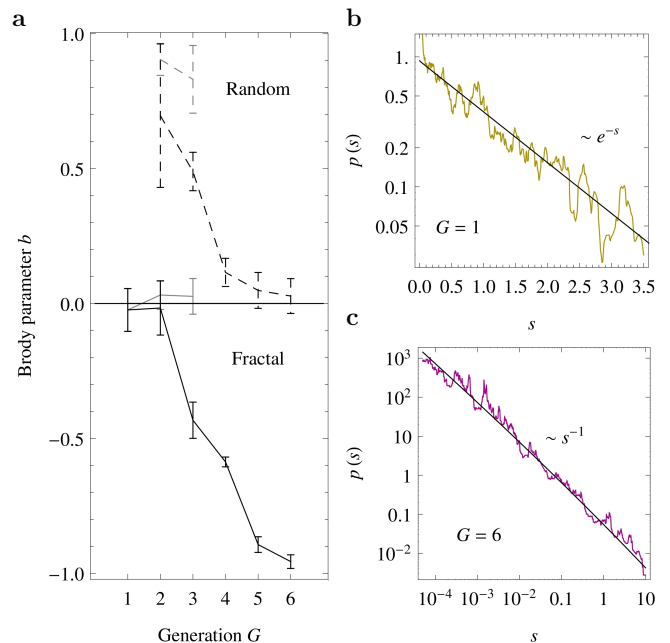

Figure 3. **a,** dependence of the Brody parameter b of the distribution of level spacings on the fractal generation G. Solid black: the low-energy regime (i) (see text) undergoes a transition from the exponential (**b,** for $G = 1$, $b \approx 0$ reflecting Poisson level statistics) to inverse power-law distribution (**c,** for $G \geq 6$, $b \approx -1$); Solid gray: the high-energy regime (ii) shows no (or at most weak) dependence on G, approximately following the Poisson distribution for all G. Dashed black: low energy regime (i) for the random fractal, evolving from the Wigner ($b \approx 1$) to exponential ($b \approx 0$) distribution; Dashed gray: regime (ii) showing no (or at most weak) dependence on $G \geq 2$.

analogous random fractal carpet, where the holes are distributed randomly without overlapping (Fig. 1), and in the equivalent regular but non-fractal geometry, where all the holes are of the same size and are distributed regularly in a lattice (Fig. 1).

The random fractal exhibits a quasi-continuous spectrum instead of the level repulsion and attraction pattern. Even if the potential well exhibits scale invariance in a statistical fashion, breaking the geometrical symmetries results in Anderson localization [29], typical of disordered media and here reflected in the localized eigenfunctions in Fig. 1. After rescaling the mode numbers and energies as for the fractal, we find the same regime at high energies $\epsilon^* > 1$ ($\mathcal{N}^* > 1$, Fig. 2d right panel). However, in this regime for $G = 2$ and 3 the Brody parameter is $b = 0.90 \pm 0.06$ and $b = 0.83 \pm 0.12$ respectively (Fig. 3), close to the value 1 characteristic of chaotic systems. On the other hand, the low-energy part of the spectrum— where Anderson states are found—lacks the band and gap structure, and the Brody parameter evolves, remarkably, from $b = 0.7 \pm 0.2$ for $G = 2$ to $b = 0.03 \pm 0.06$ for $G = 6$ as for an integrable system (see section II of SM for

details). Thus, breaking the regularity of the fractal results in the loss of the scale invariance of nearest-neighbor level spacings.

As another control, we analyzed the equivalent regular lattice of holes of equal size. This system retains the geometrical symmetries of the square but lacks the scale invariance since it has only two characteristic scales—the size of the holes and the size L of the system. We find that the spectrum of the lattice exhibits none of the remarkable properties of the fractal (scaling of the energy levels, presence of a regime with band-gap structure, self-similarity). This system must be desymmetrized in order to fit the spacings distribution to the form given by Eq. (1); the fitted distribution has a positive Brody parameter that evolves to $b \approx 0$ for the largest generations (see SM section II). *Overall, these two negative controls suggest that the unique features of the spectrum of the fractal are due to the combined effect of geometrical symmetries and scale invariance.*

The electron gas. We used 1000 single-particle states in order to study the thermodynamic properties of the non-correlated electron gas [16] in a Sierpinski carpet. The Fermi level of the system for different total number of electrons N_e with spin degeneracy is presented in Fig. 4. It is shown that the generation G can be chosen to obtain a Fermi level located close to a gap, and reproduce the properties of a semiconductor material with tailored band gap. The heat capacity $C(T)$ for $N_e = 100$ electrons is shown in Fig. 4 (see section III of SM for details). The 1000 states suffice to describe each system accurately in a window of temperatures of almost three times the Fermi temperature T_F ($T_F = \pi N_F \approx 314$ for $G = 0$). For $G = 0$ we recover the behavior of the 2D electron gas (2DEG), as expected. Indeed, $C(T)$ depends linearly on T at low temperatures and converges to the classical limit ($C_{cl} = N_e$ in two dimensions) at $T \sim 2T_F$. For $G = 1$ and $G = 2$ we obtain a similar behavior, with small deviations from the behavior of the 2DEG. However, for $G \geq 3$ the presence of quasi-continuous bands separated by large energy gaps becomes important at low temperatures, where the increasing temperature permits some electrons to suddenly cross the energy gaps and populate higher energy bands in a process that is reflected in the oscillations of the heat capacity as a function of temperature. For the highest generations, oscillations become substantial in a wider range of temperatures and, at higher temperatures, the heat capacity eventually overshoots the classical limit. Remarkably, the dependence of the heat capacity per particle on the temperature expressed in units of Fermi temperature converges to the same limit curve for the highest generations (Fig. 4).

Two different mechanisms contribute to the overshooting: On one hand, the observed oscillations due to the thermal population of high energy bands in regime (i) become more relevant as the generation increases. Figure 4 shows that for $N_e = 100$ at a temperature of $T \sim 2T_F$
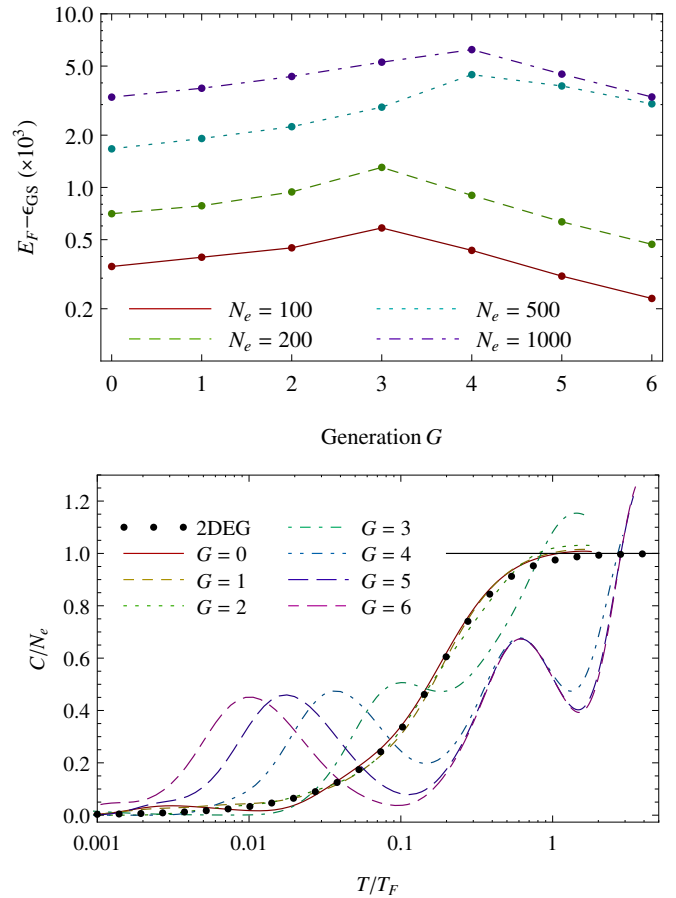

Figure 4. Top panel: Fermi energy E_F with respect the ground state energy of noninteracting electron gas for $N_e = 100, 200, 500,$ and 1000 electrons for all generations studied here. Bottom panel: Dependence of the heat capacity per particle C/N_e on temperature (in units of Fermi Temperature) T/T_F for $N_e = 100$ electrons. The alternation of bands and gaps generates oscillations in C as electrons thermally populate higher energy bands, and results in an overshooting with respect to the asymptotic thermodynamical value $C = N_e$ for a 2DEG (shown as a horizontal black line), even at temperatures where the equivalent non-fractal 2DEG has reached the classical limit. Remarkably, it converges to a well-defined function of T/T_F as the generation increases.

where the 2DEG ($G = 0$) already behaves classically, an analogous system of the same size but with the shape of a Sierpinski carpet still behaves quantum-mechanically. On the other hand, the increasing value of the ratio of the perimeter and surface of the fractal with increasing G affects the energy dependence of the density of states in regime (ii). Indeed, the first correction term to Weyl's law is proportional to the perimeter and its dependence on $\sqrt{\epsilon}$ gives rise to the overshooting (see SM section IV), this effect becoming more pronounced as the perimeter term dominates over the surface term. However, for any finite value of G, the surface contribution eventually dominates over the perimeter correction at sufficiently high energies, and thus the asymptotic value agrees with the

2D ideal-gas value. This would *not* happen in the limit $G \to \infty$ (for a fixed energy or temperature); in this limit the surface of the fractal becomes zero while the perimeter becomes infinite, yielding a non-classical result of a divergent heat capacity.

In summary, the energy spectrum of quantum particles trapped in a Sierpinski structure shows self-similarity, with level attraction and repulsion leading to bands and gaps at any scale. The distribution of consecutive energy level spacings exhibits a transition from an exponential to inverse power law density as the fractal generation increases. At high generations, no characteristic size for the spacings can be defined and level spacings of any order of magnitude are equally probable. In fractal geometries, quantum effects originating from the discreteness of the energy levels can be observed at temperatures where the equivalent non-fractal system already behaves classically.

In view of our results, fractal-shaped wires could exhibit promising features for a wide range of applications. Scale invariance of the spectrum could improve the photoelectric interaction of nanodevices in a wide range of light frequencies and allow the design of nanomaterials with tailored Fermi levels, band gaps, and conduction bands that can be thermally populated—mimicking the properties of semiconductors, as seen in the oscillations of the heat capacity—with potential applications for solar cells [30, 31], artificial photosynthesis [32], or metamaterials [4, 5, 13, 33]. In addition, the persistence of quantum effects at high temperatures could increase the operating temperature range of these quantum nanodevices.

---

* alberto.hernandodecastro@epfl.ch

† jiri.vanicek@epfl.ch

[1] G. Cao and Y. Wang, in *World Scientific Series in Nanoscience and Nanotechnology: Volume 2*, edited by F. Spaepen (World Scientific, Singapore, 2011) 2nd ed.

[2] J. Stangl, V. Holy, and G. Bauer, Rev. Mod. Phys. **76**, 725 (2004).

[3] R. Hohlfeld and N. Cohen, Fractals **7**, 79 (1999).

[4] X. Huang, Opt. Express **18**, 10377 (2010).

[5] N. Cohen, Fractals **20**, 227 (2012).

[6] M. Fairbanks, *Transposrt in micro to nanoscale solid state networks*, Ph.D. thesis, University of Oregon (2010).

[7] J. Pollanen, J. Li, C. Collet, W. Gannon, W. Halperin, and J. Sauls, Nature Phys. **8**, 317 (2012).

[8] R. Batabyal., J. Appl. Phys. **114**, 064304 (2013).

[9] M. Massicotte., Nanotechnology **24**, 325601 (2013).

[10] D. Hofstadter, Phys. Rev. B **14**, 2239 (1976).

[11] B. H. et al., Science **340**, 1427 (2013).

[12] G. N. Katomeris and S. N. Evangelou, J. Phys. A: Math. Gen. **29**, 2379 (1996).

[13] G. Volpe, G. Volpe, and R. Quidant, Opt. Lett. **19**, 3612 (2011).

[14] P. J. Richens and M. V. Berry, Physica D **2**, 495 (1981).

[15] A. Hernando and J. Vaníček, Phys. Rev. A **88**, 062107 (2013).

[16] L. Girifalco, *Statistical Mechanics of Solids* (Oxford Univ. Press, Oxford, 2000).

[17] L. Reichl, *The Transition to Chaos: Conservative Classical Systems and Quantum Manifestations*, 2 ed. (Springer-Verlag, New York, 2004).

[18] A. Edelman and N. Rao, Acta Numer. **14**, 233 (2005).

[19] T. A. Brody, J. Flores, J. B. French, P. A. Mello, A. Pandey, and S. S. M. Wong, Rev. Mod. Phys. **53**, 385 (1981).

[20] M. V. Berry and M. Tabor, Proc. Royal Soc. London A **356**, 375 (1977).

[21] S. W. McDonald and A. N. Kaufman, Phys. Rev. Lett. **42**, 1189 (1979).

[22] M. V. Berry, Annals of Phys. **131**, 163 (1981).

[23] O. Bohigas, M. J. Giannoni, and C. Schmit, Phys. Rev. Lett. **52**, 1 (1984).

[24] T. H. Seligman, J. J. M. Verbaarschot, and M. R. Zirnbauer, Phys. Rev. Lett. **53**, 215 (1984).

[25] M. V. Berry and M. Robnik, J. Phys. A: Math. Gen **17**, 24413 (1984).

[26] J. Sakhr and J. M. Nieminen, Phys. Rev. E **72**, 045204(R) (2005).

[27] Y. Alhassid, A. Novoselsky, and N. Whelan, Phys. Rev. Lett. **65**, 2971 (1990).

[28] T. Geisel, R. Ketzmerick, and G. Petschel, Phys. Rev. Lett. **66**, 1651 (1991).

[29] P. Anderson, Phys. Rev. **109**, 1492 (1958).

[30] L.-H. Zhu, M.-R. Shao, R.-W. Peng, R.-H. Fan, X.-R. Huang, and M. Wang, Opt. Express **21**, A313 (2013).

[31] S. Abdellatif and K. Kirah, Opt. Lett. **38**, 3680 (2013).

[32] X. Wang, K. Maeda, A. Thomas, K. Takanabe, G. Xin, J. M. Carlsson, K. Domen, and M. Antonietti, Nature Materials **8**, 76 (2009).

[33] D. Schurig, J. Mock, B. Justice, S. Cummer, J. Pendry, A. Starr, and D. Smith, Science **314**, 977 (2006).